ChemComm

COMMUNICATION

View Article Online
View Journal | View Issue



Cite this: *Chem. Commun.*, 2021, 57, 1153

Received 28th October 2020,
Accepted 22nd December 2020

DOI: 10.1039/d0cc07142k

rsc.li/chemcomm

# Increasing the activity of the $Cu/CuAl_2O_4/Al_2O_3$ catalyst for the RWGS through preserving the $Cu^{2+}$ ions†

Ali M. Bahmanpour, [a] Benjamin P. Le Monnier,[a] Yuan-Peng Du, [a] Florent Héroguel, [a] Jeremy S. Luterbacher [a] and Oliver Kröcher [a]*[ab]

**Cu–Al spinel oxide is a highly active catalyst for $CO_2$ conversion to CO. However, it suffers from low surface area. By depositing a silica layer, we protected the catalyst surface and preserved the $Cu^{2+}$ ions during the calcination process. These ions form well-dispersed Cu sites which participate in the reaction.**

Reducing fossil-derived carbon dioxide emissions and their associated environmental effects is one of today's major challenges. Carbon recycling is more vital than ever in order to limit global warming and the resulting climate change.[1,2] In addition, $CO_2$ is a cheap source of carbon, the efficient usage of which can ensure a secure sustainable economy. Therefore, mitigation of $CO_2$ and its conversion to value-added chemicals has been the objective of many research projects.

Methanol is an important bulk chemical that can be produced through direct conversion of $CO_2$. However, due to the low activity and high thermal stability of $CO_2$, only low yields are obtained. In contrast, synthesis of methanol and other chemicals from CO is well-established and well-studied.[3,4] In many of the direct $CO_2$ hydrogenation routes to chemicals, CO is actually formed as a reaction intermediate.[5,6] The hydrogenation of $CO_2$ to CO is known as the reverse water gas shift reaction (RWGSR) and has gained more attention in recent years. Noble metal-based catalysts have shown high activity towards this reaction. However, due to their high cost, efforts have been focused on finding an inexpensive substitute. $Cu/ZnO/Al_2O_3$ can actively catalyse the reaction. However, it suffers from severe deactivation.[7,8] Recently, we have demonstrated that copper aluminate ($CuAl_2O_4$, spinel structure) is as an active catalyst for the RWGSR.[7,9] This catalyst is commonly prepared through co-precipitation of the constituting metal precursors followed by a high-temperature calcination step ($\geq 900$ °C). The high temperature causes the reaction of Cu and $Al_2O_3$ to form $CuAl_2O_4$ but it also leads to particle sintering and a low surface area.[10] Variation of the chemical composition of the support has been used as another method for preserving metal ions and particles on the catalyst surface.[11,12] Another way to inhibit particle sintering is to deposit a protective layer on the catalyst surface.[13,14] In most cases, the protective layer acts as a physical barrier, which immobilizes the nanoparticles.[15,16] In some cases, it also alters the chemical properties of the support or even enhances the overall catalyst activity due to advantageous changes of the catalyst structure[13,14] despite the layer covering some of the active sites. Layer deposition techniques could be improved by several strategies to inhibit or suppress site blockage, which can minimize this negative effect.[17,18]

In this study, we added a silica layer through a controlled surface sol–gel method to protect Cu nanoparticles impregnated on $Al_2O_3$ during the high temperature calcination step that forms the desired copper aluminate phase (catalyst labelled as CuAlSi-900). The schematic is shown in Fig. 1a. In order to study the effect of the silica layer's addition, we have also prepared a control catalyst using the same procedure without depositing the silica layer (catalyst labelled as CuAl-900). The experimental methods for catalyst preparation are described fully in the (ESI†). The EDSX-STEM image (Fig. 1b) shows the successful deposition of a uniform silica layer as well as the high dispersion of the Cu particles. The image for CuAl-900 is presented in the ESI,† (Fig. S1).

The catalyst activities for $CO_2$ hydrogenation to CO are shown in Fig. 2. By depositing a silica layer, not only did the initial activity of the catalyst not deteriorate due to the potential blockage of some of the active sites, but appears to have been enhanced by about 10% compared to the control catalyst. The stability of the CuAlSi-900 catalyst is presented in Fig. S2 (ESI†) and its activity is compared with other catalysts in the literature (Table S1, ESI†). The reproducibility of the catalyst syntheses

[a] *Institute of Chemical Sciences and Engineering, École Polytechnique Fédérale de Lausanne (EPFL), Lausanne 1015, Switzerland*
[b] *Paul Scherrer Institut (PSI), Villigen 5232, Switzerland. E-mail: oliver.kroecher@psi.ch*

† Electronic supplementary information (ESI) available: Experimental details, catalyst characterization data, XRD patterns, XPS spectra, and $N_2$ physisorption data. See DOI: 10.1039/d0cc07142k

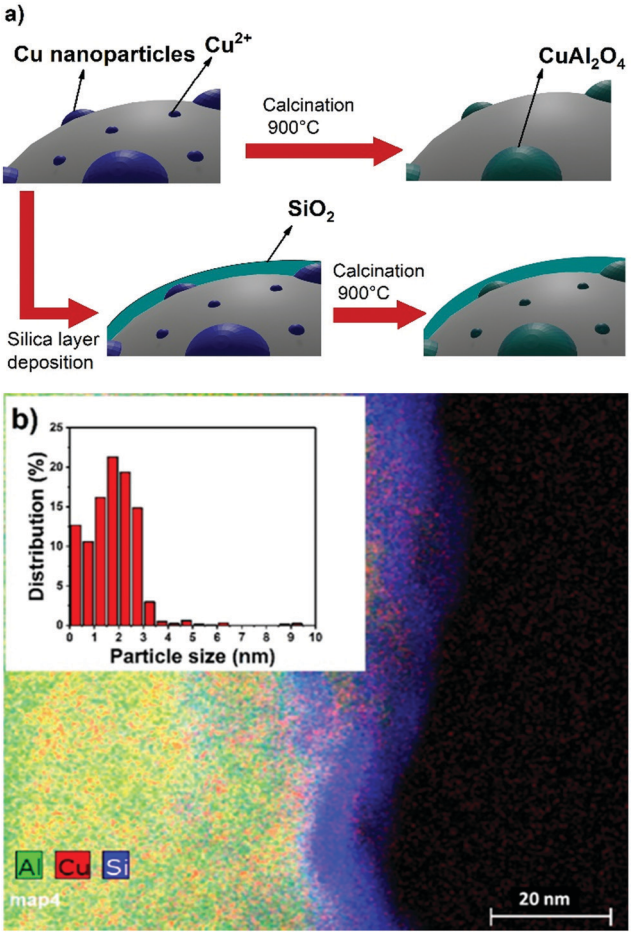


Fig. 1 (a) Schematic presentation of the catalyst preparation process. (b) STEM and particle size distribution of the CuAlSi-900 catalyst.

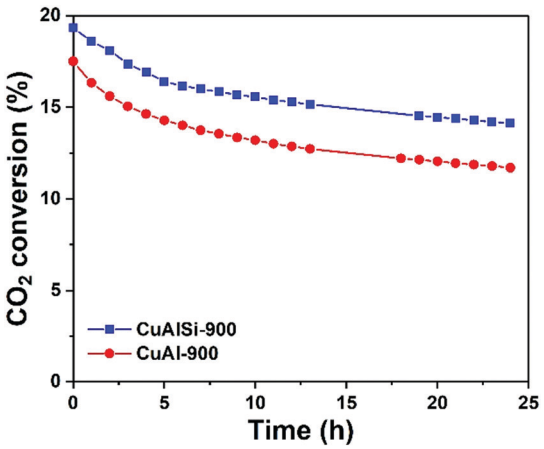


Fig. 2 Catalyst activity of CuAl-900 and CuAlSi-900. $T$ = 450 °C, $P$ = 1 bar, WHSV = 15 000 mL $g^{-1}$ $h^{-1}$.

and activity tests was checked and the second set of results closely matched the first (Fig. S3, ESI†). This confirmed the protective effect of the silica layer and proved the reliability and low sensitivity of the preparation method, which is important for its potential application in industrial processes. The catalyst samples were further characterized to identify the source of the higher activity.

X-ray diffraction (XRD) measurements (Fig. S4, ESI†) did not show any Cu-based crystals, which implied that the most of the nanoparticles were smaller than the detection threshold (*ca.* 2 and 3 nm), which was confirmed by the Cu particles size distribution determined by multiple images analysis using ImageJ software (Fig. 1b, inset). However, the XRD patterns did show the formation of α-alumina peaks on the control catalyst CuAl-900. Therefore, high temperature treatment partly converted γ-alumina into α-alumina. This phenomenon did not occur on CuAlSi-900, presumably due to the presence of the protective silica layer which acted as a stabilizer for γ-alumina.[19,20]

α-alumina is known to have a lower surface area compared to γ-alumina.[21] Therefore, deposition of the protective silica layer helped to maintain the surface area of the catalyst as was further verified using $N_2$ physisorption (Fig. S5 and Table S2, ESI†). The BET surface area of both catalysts before the high-temperature calcination was similar (~116 $m^2$ $g^{-1}$). The pore volume of the CuAlSi catalyst was lower compared to CuAl (0.13 mL $g^{-1}$ as opposed to 0.22 mL $g^{-1}$) since the non-calcined deposited silica layer potentially plugged some of the pores (5 and 6 nm pore range, Fig. S6, ESI†). However, after calcination at 900 °C the BET surface area of CuAl-900 catalyst dropped to 63 $m^2$ $g^{-1}$, presumably due to the sintering of the γ-alumina crystals and formation of the low-surface area α-alumina. In contrast, for the CuAlSi-900 catalyst, the surface area dropped only to 85 $m^2$ $g^{-1}$. We attributed the higher surface area of the CuAlSi-900 to the inhibition of the formation of low-surface area α-alumina crystals as well as the protection of the γ-alumina crystals from sintering, which can be inferred from the lower intensity of the γ-alumina crystal peaks in its XRD pattern compared to the CuAl-900 catalyst (Fig. S4, ESI†). Moreover, the pore volume of the CuAlSi-900 increased to 0.17 mL $g^{-1}$ after calcination of the silica layer, which might have cracked the overcoat, creating larger pores (Fig. S6, ESI†), or removed leftover organic precursors, while the CuAl-900 lost some of its pore volume (0.19 mL $g^{-1}$ after calcination, Table S2, ESI†).

X-ray photoelectron spectroscopy (XPS) was applied in order to study the potential formation of $CuAl_2O_4$ on the catalyst surfaces (Fig. S7, ESI†). For both catalysts, the same surface Cu/Al molar ratio (0.012) was found (Table S2, ESI†). We also noted the presence of tetrahedral coordinated Cu on the surface of both catalysts (the binding energy of ~935 eV on Cu 2p), which confirms the presence of the $CuAl_2O_4$ phase.[22]

In an attempt to identify the Cu species on both catalysts, temperature-programmed reduction ($H_2$-TPR) tests (Fig. 3a) and electron paramagnetic resonance (EPR) tests (Fig. 3b) were conducted. Three peaks were identified through $H_2$-TPR tests for both catalysts. The first peak (~250–310 °C) is assigned to the reduction of very well-dispersed Cu–O entities and the second peak (~550 °C) is assigned to reduction of CuO in the bulk. The third peak (~670–740 °C) is assigned to the

 

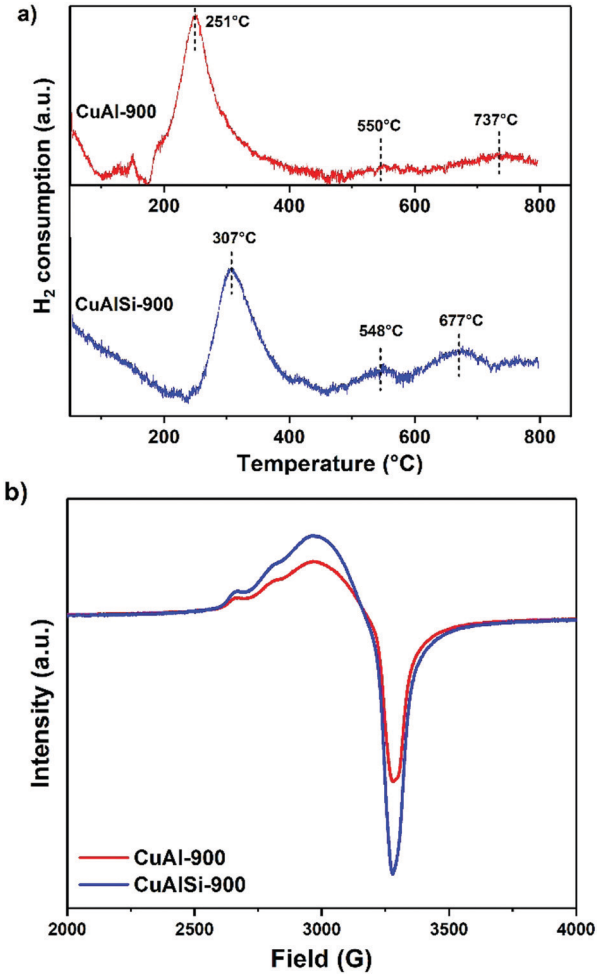


Fig. 3 (a) $H_2$-TPR profiles and (b) EPR spectra for CuAl-900 and CuAlSi-900 catalysts.

reduction of the $CuAl_2O_4$ phase in both catalysts.[23,24] The formation of the well-dispersed Cu–O entities is known to be either caused by isolated $Cu^{2+}$ ions, which are present on the catalyst surface and strongly interact with their support due to their ionic character, or by weak magnetic associates, or two- or three-dimensional Cu clusters.[25] For the sample with the surface silica layer, the peak in the TPR profile representing the well-dispersed Cu–O entities appeared at higher temperatures (251 °C in CuAl-900 and 307 °C in CuAlSi-900) while the third peak, which represents the reduction of the $CuAl_2O_4$ phase, shifted to lower temperatures (from 737 °C in CuAl-900 to 677 °C in CuAlSi-900). The apparent upward shift of the peak for well-dispersed Cu–O shows the reluctance of these entities to react with hydrogen due to their stronger interaction with $CuAl_2O_4$. This implies that, unlike CuAl-900 catalyst, this peak is mostly caused by the isolated $Cu^{2+}$ ions on this catalyst rather than the weak magnetic associates, or two- and three- dimensional clusters. Therefore, the appearance of this peak at higher temperatures is due to the higher contribution of the isolated $Cu^{2+}$ ions on the CuAlSi-900 catalyst surface since they are more prominent. This is found to be a dispersion effect and not a new site creation. The downward shift of the peak for $CuAl_2O_4$ reduction to lower temperatures shows the higher reducibility of $CuAl_2O_4$ due to the spillover effect caused by the higher interaction of $CuAl_2O_4$ with the isolated $Cu^{2+}$ ions forming well-dispersed and small Cu islands after reduction.[26,27] This phenomenon shows that there is a strong interaction between copper ions and the copper aluminate that was formed.

To confirm this hypothesis, we used EPR to characterise the catalyst. The hyperfine structure, which appears due to the lack of spin–spin interaction, is almost equally well-resolved for both samples indicating that the $Cu^{2+}$ ions, which are present on both catalysts, are isolated. This is in line with the relatively low Cu loading for both samples (1 wt%), which helps ion dispersion. Whereas the degree of isolation of the $Cu^{2+}$ ions is comparable for both catalysts, the higher intensity of the spectra of CuAlSi-900 reveals a higher concentration of $Cu^{2+}$ ions in this sample. This means that the isolated $Cu^{2+}$ ions were better preserved in the CuAlSi-900 catalyst during the high-temperature calcination process, probably due to the effect of the interfacial sites.

In our previous study, we had shown that the $CuAl_2O_4$ phase leads to particularly favourable $CO_2$ adsorption and that most of the adsorbed $CO_2$ molecules remain on the $CuAl_2O_4$ surface as spectators due to their strong adsorption on the oxygen vacancies.[9] Only the adsorbed $CO_2$ intermediates (either in form of carbonates or formates) which are adsorbed next to surface hydrogen will be further hydrogenated and desorb from the catalyst surface as CO.[28,29] Therefore, we suggest that the role of the isolated surface $Cu^{2+}$ ions is to form highly dispersed metallic Cu entities, which act as the $H_2$ binding sites during the reaction. Since the reaction temperature was kept at 450 °C, and based on our $H_2$-TPR results, the isolated $Cu^{2+}$ ions were likely reduced under operation conditions. In order to test the effect of these dispersed ions, a temperature-programmed surface reaction (TPSR) was conducted using the CuAlSi-900 catalyst (Fig. 4). In one test, the catalyst was only activated under Ar at 300 °C to avoid $Cu^{2+}$ reduction while in the other test, the catalyst was pre-reduced using a $H_2$/Ar flow at 400 °C before the test. When the catalyst was not pre-reduced, the formation of CO started at ~268 °C (Fig. 4a), which almost matches the start of the first reduction peak of $H_2$-TPR experiment. For the pre-reduced catalyst (Fig. 4b), however, the CO evolution starts already at ~228 °C. We surmise that, since the $Cu^{2+}$ ions were already reduced, they could facilitate the reaction at these lower temperatures. Based on the $H_2$-TPR profiles, the bulk CuO and the $CuAl_2O_4$ phase were likely not reduced at this temperature. Therefore, the active sites of the CuAlSi-900 catalyst are consisted of $CuAl_2O_4$, which were found to be active in $CO_2$ adsorption, as well as dispersed $Cu^0$ entities, active for $H_2$ adsorption and dissociation, which formed due to the reduction of the $Cu^{2+}$ ions on the catalyst surface during the reaction.

The formation of high-surface area $CuAl_2O_4$ phase, also known as the Cu–Al spinel oxide phase, which act as strong $CO_2$ adsorption sites, is complicated by the high-temperature calcination step which causes severe sintering. Here, we have

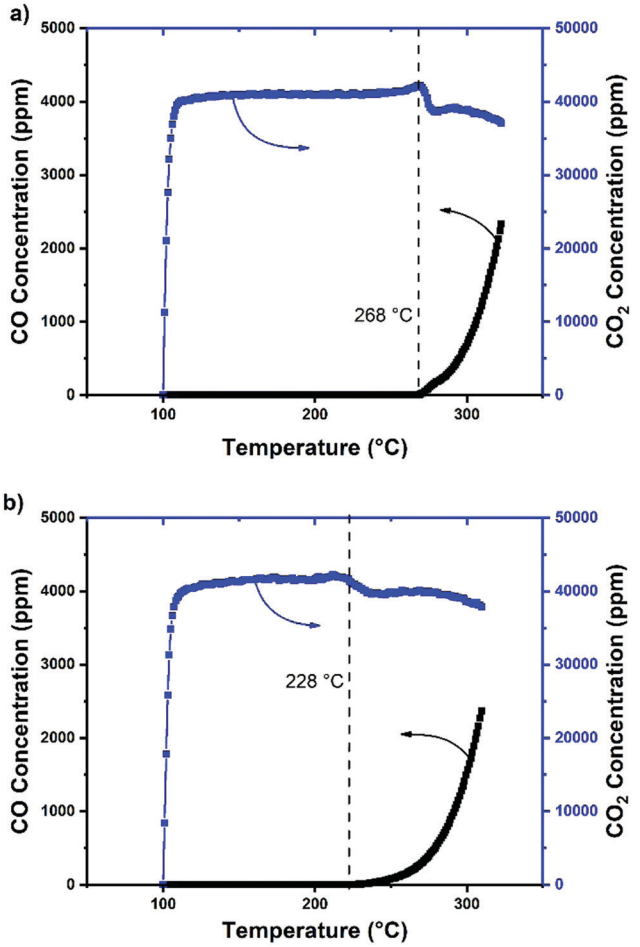


Fig. 4 TPSR test for CuAlSi-900 (a) without pre-reduction and (b) with pre-reduction of the catalyst at 400 °C.

used a silica layer as a protective overcoat for this step in order to maintain the surface area of the catalyst. We observed that not only was the surface area partly preserved after calcination by using the protective layer, but the well-dispersed, isolated $Cu^{2+}$ ions also saw their stability increase during the calcination step. These ions were then reduced during the reaction to form Cu entities, which acted as adsorbed $H_2$ sources for the activation of the adsorbed $CO_2$ on the $CuAl_2O_4$ surface.

This research project is part of the Swiss Competence Center for Energy Research SCCER BIOSWEET of the Swiss Innovation Agency Innosuisse. JSL, BPLM and YPD were supported by the European Research Council (ERC) under the European Union's Horizon 2020 research and innovation program (Starting grant: CATACOAT, No 758653). The authors would like to acknowledge Dr Mounir Mensi for XPS analysis, Dr Pascal Schouwink for XRD analysis, Dr Andrzej Sienkiewicz for EPR analysis, Mr Kasper Sohald for his assistance with the experiments, and Mr Sylvain Coudret for ICP-OES analysis.

## Conflicts of interest

There are no conflicts to declare.

## Notes and references

1 W. Wang, S. Wang, X. Ma and J. Gong, *Chem. Soc. Rev.*, 2011, **40**, 3703–3727.
2 J. C. Zachos, G. R. Dickens and R. E. Zeebe, *Nature*, 2008, **451**, 279–283.
3 G. C. Chinchen, P. J. Denny, J. R. Jennings, M. S. Spencer and K. C. Waugh, *Appl. Catal.*, 1988, **36**, 1–65.
4 R. G. Herman, K. Klier, G. W. Simmons, B. P. Finn, J. B. Bulko and T. P. Kobylinski, *J. Catal.*, 1979, **56**, 407–429.
5 J. H. Kwak, L. Kovarik and J. Szanyi, *ACS Catal.*, 2013, **3**, 2094–2100.
6 I. A. Fisher and A. T. Bell, *J. Catal.*, 1996, **162**, 54–65.
7 A. M. Bahmanpour, F. Héroguel, M. Kılıç, C. J. Baranowski, L. Artiglia, U. Röthlisberger, J. S. Luterbacher and O. Kröcher, *ACS Catal.*, 2019, **9**, 6243–6251.
8 X. Zhang, X. Zhu, L. Lin, S. Yao, M. Zhang, X. Liu, X. Wang, Y.-W. Li, C. Shi and D. Ma, *ACS Catal.*, 2017, **7**, 912–918.
9 A. M. Bahmanpour, F. Héroguel, M. Kılıç, C. J. Baranowski, P. Schouwink, U. Röthlisberger, J. S. Luterbacher and O. Kröcher, *Appl. Catal., B*, 2020, **266**, 118669.
10 G. Li, C. Gu, W. Zhu, X. Wang, X. Yuan, Z. Cui, H. Wang and Z. Gao, *J. Cleaner Prod.*, 2018, **183**, 415–423.
11 T. Sun, P. Zhang, W. Chen, K. Wang, X. Fu, T. Zheng and J. Jiang, *Chem. Commun.*, 2020, **56**, 798–801.
12 T. Sun, Y. Li, T. Cui, L. Xu, Y.-G. Wang, W. Chen, P. Zhang, T. Zheng, X. Fu, S. Zhang, Z. Zhang, D. Wang and Y. Li, *Nano Lett.*, 2020, **20**, 6206–6214.
13 S. H. Krishna, L. Zhang, I. Hermans, G. W. Huber, T. F. Kuech and J. A. Dumesic, *J. Catal.*, 2020, **389**, 111–120.
14 L. Cao and J. Lu, *Catal.: Sci. Technol.*, 2020, **10**, 2695–2710.
15 H. O. Otor, J. B. Steiner, C. García-Sancho and A. C. Alba-Rubio, *ACS Catal.*, 2020, **10**, 7630–7656.
16 B. P. Le Monnier, F. Wells, F. Talebkeikhah and J. S. Luterbacher, *Adv. Mater.*, 2019, **31**(52), 1904276.
17 T. Van Cleve, D. Underhill, M. Veiga Rodrigues, C. Sievers and J. W. Medlin, *Langmuir*, 2018, **34**, 3619–3625.
18 F. Liu, C. Okolie, R. M. Ravenelle, J. C. Crittenden, C. Sievers, P. C. A. Bruijnincx and B. M. Weckhuysen, *Appl. Catal., A*, 2018, **551**, 13–22.
19 Y. Saito, T. Takei, S. Hayashi, A. Yasumori and K. Okada, *J. Am. Ceram. Soc.*, 1998, **81**, 2197–2200.
20 T. Chopin, G. Dovergne and J.-L. Le Loarer, *US Pat.*, US5273949A, 1993.
21 D. S. Maciver, H. H. Tobin and R. T. Barth, *J. Catal.*, 1963, **2**, 485–497.
22 R. B. Mane and C. V. Rode, *Green Chem.*, 2012, **14**, 2780–2789.
23 M. Jabłońska, *Chem. Pap.*, 2015, **69**, 1141–1155.
24 M. Jabłońska, A. M. Beale, M. Nocuń and R. Palkovits, *Appl. Catal., B*, 2018, **232**, 275–287.
25 W.-P. Dow, Y.-P. Wang and T.-J. Huang, *J. Catal.*, 1996, **160**, 155–170.
26 M.-S. Kim, S.-H. Chung, C.-J. Yoo, M. S. Lee, I.-H. Cho, D.-W. Lee and K.-Y. Lee, *Appl. Catal., B*, 2013, **142–143**, 354–361.
27 F. Liao, Y. Huang, J. Ge, W. Zheng, K. Tedsree, P. Collier, X. Hong and S. C. Tsang, *Angew. Chem., Int. Ed.*, 2011, **50**, 2162–2165.
28 L. F. Bobadilla, J. L. Santos, S. Ivanova, J. A. Odriozola and A. Urakawa, *ACS Catal.*, 2018, **8**, 7455–7467.
29 X. Wang, H. Shi, J. H. Kwak and J. Szanyi, *ACS Catal.*, 2015, **5**, 6337–6349.

 